Thermochimica Acta, 239 (1994) 33–40
Elsevier Science B.V., Amsterdam
SSDI 0040-6031(93)01644-I

Thermodynamic properties of K_2ZnCl_4 between 5 and 350 K

J.C. van Miltenburg [a,*], I. Noiret [b] and A. Hedoux [b]

[a] *Department of Interfaces and Thermodynamics, State University of Utrecht, Padualaan 8, 3508 TB Utrecht, The Netherlands*
[b] *Laboratoire de Dynamique en Structure de Materiaux Moleculaires, CNRS URA 801, Universite de Lille 1, U.F.R. de Physique. Bât. P5, 59655 Villeneuve D'Ascq Cédex, France*

(Received 18 October 1993; accepted 7 November 1993)

Abstract

The low-temperature heat capacities of K_2ZnCl_4 were measured between 5 and 350 K. A phase transition with a heat effect of 30 J mol^{-1} was found at 144 K. Between the transition temperature and 210 K, the sample shows a slow transformation which is probably related to the distortions of the $ZnCl_4$ tetrahedra. This is in accordance with Raman and DSC experiments. The thermodynamic properties of a compound are given at rounded temperatures.

INTRODUCTION

The successive structural phase transitions Normal (**N**)–INCommensurate (**INC**)–Commensurate (**C**) in A_2BX_4 compounds (where A is Rb, K, etc., B is Zn, Se, Co, etc., and X is Cl, Br, etc.) have been the subject of a great deal of attention. Commonly, an intermediate **INC** phase is found between a para-electric phase (**N**) and a ferro-electric phase (**C**). This **INC** phase is principally described by distortions of the BX_4 tetrahedra, corresponding to rotations around the *c* and *a* crystallographic directions [1–4] (*Pmcn* being the space group of the basic structure). As a consequence, the characteristics of the temperature dependence of modulation, which induces the sequence of modulated phases, corresponds to the temperature behaviour of the tetrahedron distortions. These distortions induce a modulation of the basic lattice, characterized by the wave vector $\mathbf{q} = (\frac{1}{3} - \delta)\mathbf{c}^*$. In the **INC** phase, δ is temperature dependent and becomes equal to zero at the lock-in transition.

Below the lock-in transition, the number and the nature of the phase transitions found in the different compounds of the A_2BX_4 family differ. In

* Corresponding author.

K_2SeO_4, no further phase transitions have been observed below the lock-in temperature. A second-order phase transition associated with a soft mode has been found at 74.6 K for Rb_2ZnCl_4 [5, 6] and at 111.7 K for Rb_2ZnBr_4, which undergoes a further second-order phase transition at 76.5 K [7]. In K_2ZnCl_4 ($T_{N-INC} = 553$ K, $T_{INC-C} = 403$ K), neutron diffraction [8], dielectric [9] and a.c. calorimetric [9] experiments have revealed a new incommensurate phase between 144.5 and 148 K, whereas heat capacity measurements have shown only a first-order phase transition at about 146 K. More recent studies [10] have revealed a slow transformation of the distortions of the $ZnCl_4$ tetrahedron at about 250 K, by observation of the splitting of a Zn–Cl stretching mode (with Raman spectroscopy) and of a broad enthalpic effect (DSC). Moreover, at a lower temperature (about 105 K), a splitting of the low-frequency Raman-active modes in the totally symmetric representation was observed [11]. In order to understand the successive phase transitions below the common sequence **N–INC–C** and to try to clarify the time-dependent phenomena just above the transition at 146 K, heat capacity measurements were made for K_2ZnCl_4 between 5 and 350 K.

EXPERIMENTAL

Single crystals of K_2ZnCl_4 were grown by slow evaporation of a solution containing KCl and a slight excess of $ZnCl_2$. The crystals were crushed slightly and dried under vacuum.

The calorimeter (cal V) and its measuring system were described previously [12]. The calorimeter vessel (12 ml capacity) is made of gold-plated electrodeposited copper, with a re-entrant well for the thermometer–heater assembly. The 100 Ω platinum thermometer was calibrated between 13 and 300 K by the N.P.L. (England), based on the IPTS-68 temperature scale. A sample mass of 12.221 g, corresponding to 0.04282 mole (using a molar mass of 285.397 g mol^{-1}) was loaded under nitrogen into the vessel, and then the vessel was evacuated for about an hour. Helium (2000 Pa) was admitted to serve as a heat exchange gas and the vessel was closed.

We suspect that the thermal history can be important for the transition. Therefore, a detailed account of this, together with the stabilization and input times and the mean heating rate during the run is given in Table 1. The experimental data are given in chronological order in Table 2 and are plotted in Fig. 1.

In the first measurement (between 80 and 220 K), the transition around 145 K is sharp; from this transition to about 210 K, the sample shows an increasing negative temperature drift during the stabilization periods, peaking at 180 K and levelling off to a normal value at 210 K. The series 2–6 cover the range between 5 and 158 K. Series 6 passes very slowly through the transition, without showing exceptional heat effects afterwards. Series 7 remeasures the region covered by series 1. Once again, irregular behaviour

TABLE 1

Thermal history of the sample and measuring conditions of series

Series	T_{start}/K	$t_{stabilization}$/s	t_{input}/s	Mean heating rate/K h^{-1}	T_{end}/K	Time at T_{end}/h	Time to cool to next series/h
Start	−300	–	–	–	300	24	2
1	79	600	600	6	220	15	–
2	5	120	100	20–25	34	0.1	1
3	5	100	100	20–25	35	0.1	–
4	35	410	400	7–8.5	89	12	–
5	92	1200	600	4.3	133	12	–
6	135	450	300	0.98	160	–	2
7	93	1200	900	6	306	36	–
8	293	1200	900	5	370	–	–

TABLE 2

Experimental heat capacities of K_2ZnCl_4

T/K	C_p/J K^{-1} mol^{-1}	T/K	C_p/J K^{-1} mol^{-1}	T/K	C_p/J K^{-1} mol^{-1}	T/K	C_p/J K^{-1} mol^{-1}
Series 1		137.86	153.05	32.12	46.37	45.40	72.33
79.19	115.92	139.87	154.57	33.34	48.71	47.15	75.34
81.41	117.99	141.89	157.52			48.91	78.34
83.58	119.69	143.89	162.74	Series 3		50.58	80.99
85.71	121.25	145.91	156.29	5.61	0.89	52.47	83.99
87.80	122.83	147.97	155.61	7.02	1.65	54.27	86.74
89.85	124.65	150.03	156.08	8.15	2.71	56.08	89.46
91.87	126.29	152.07	156.56	9.60	4.06	57.91	92.04
93.86	127.84	154.11	157.06	11.33	5.46	59.75	94.54
95.84	129.28	156.14	157.52	13.20	7.77	61.60	96.91
97.81	130.64	158.18	158.03	15.01	11.42	63.46	99.17
99.78	131.95	160.21	158.48	16.84	14.65	65.32	101.38
101.77	133.58			18.89	18.46	67.20	103.54
103.75	134.82	Series 2		21.11	23.04	69.08	105.66
105.73	136.03	5.15	0.96	23.40	27.81	70.97	107.62
107.72	137.21	6.19	0.91	25.53	32.44	72.86	109.58
109.72	138.38	7.45	2.04	27.36	36.15	74.78	111.29
111.71	139.57	8.71	3.26	28.97	39.51	76.70	113.33
113.71	140.72	10.12	4.52	30.44	42.33	78.61	115.12
115.71	141.80	11.94	6.00	31.78	44.95	80.53	116.83
117.72	142.87	13.80	9.08	33.02	47.29	82.46	118.55
119.72	143.95	15.55	12.40	34.19	49.18	84.40	120.19
121.73	144.96	17.45	15.76			86.34	121.65
123.74	146.00	19.56	19.83	Series 4		88.29	123.39
125.75	146.95	21.79	24.38	35.44	53.50		
127.76	147.88	24.03	29.19	37.00	56.71	Series 5	
129.78	148.88	26.06	33.66	38.58	59.92	92.81	126.88
131.80	149.83	27.81	37.53	40.27	63.12	95.26	128.65
133.82	150.86	29.39	40.73	41.96	66.32	97.68	130.30
135.83	151.86	30.81	43.74	43.68	69.39	100.06	131.94

TABLE 2 (continued)

T/K	C_p/J K^{-1} mol^{-1}	T/K	C_p/J K^{-1} mol^{-1}	T/K	C_p/J K^{-1} mol^{-1}	T/K	C_p/J K^{-1} mol^{-1}
102.41	133.72	142.15	157.93	102.84	134.03	263.41	175.96
104.72	135.20	142.35	158.74	106.70	136.46	266.45	176.19
107.00	136.57	142.56	159.14	110.58	138.83	269.48	176.55
109.27	137.92	142.76	159.77	114.48	141.11	272.51	176.89
111.50	139.27	142.96	160.79	118.36	143.26	275.53	177.22
113.71	140.54	143.16	161.58	122.19	145.25	278.55	177.35
115.90	141.79	143.37	162.55	125.95	147.11	281.56	177.73
118.06	142.94	143.57	163.84	129.67	148.90	284.57	178.11
120.21	144.05	143.77	165.01	133.33	150.66	287.57	178.41
122.33	145.11	143.98	165.09	136.95	152.51	290.56	178.62
124.44	146.19	144.18	164.33	140.51	155.37	293.55	178.94
126.53	147.20	144.39	163.13	144.02	160.02	296.53	179.25
128.60	148.18	144.59	161.61	147.51	155.47	299.51	179.62
149.13	150.74	144.80	159.85	151.01	156.05	302.49	179.89
132.70	150.11	145.00	158.49	154.48	156.82	305.47	180.16
		145.21	157.67	157.93	157.63		
Series 6		145.41	156.39	161.35	158.51	Series 8	
135.83	151.50	145.62	156.06	164.76	159.36	294.57	178.95
136.03	151.99	145.83	155.90	168.14	160.18	297.51	179.33
136.23	151.94	146.03	155.65	171.50	160.93	300.49	179.59
136.44	152.11	146.24	155.65	174.84	161.69	303.47	179.86
136.64	152.23	146.44	155.14	178.17	162.44	306.44	180.15
136.85	152.25	146.64	155.59	181.48	163.14	309.41	180.31
137.05	152.14	146.85	155.38	184.77	163.83	312.38	180.66
137.25	152.11	147.05	155.45	188.05	164.51	315.34	180.90
137.46	152.32	147.26	155.42	191.31	165.19	318.29	181.36
137.66	152.31	147.46	155.30	194.56	165.83	321.25	181.64
137.87	152.14	147.67	155.57	197.80	166.40	324.20	181.83
138.07	152.55	147.87	155.50	201.02	166.89	327.14	182.16
138.27	152.59	148.08	155.69	204.23	167.39	330.08	182.49
138.48	153.22	148.28	155.57	207.43	167.96	333.01	182.73
138.68	153.08	148.49	155.90	210.62	168.50	335.93	182.99
138.88	153.82	148.69	155.79	213.80	169.18	338.85	183.26
139.09	153.41	148.90	155.70	216.97	169.69	341.76	183.49
139.29	153.88	149.10	155.84	220.12	170.22	344.67	183.69
139.50	153.92	149.31	156.02	223.27	170.66	347.58	183.97
139.70	153.93	149.94	155.98	226.40	171.15	350.49	184.29
139.91	154.41	149.72	156.20	229.53	171.69	353.39	184.51
140.11	154.90	149.92	156.10	232.65	172.10	356.29	184.80
140.31	154.63	150.13	156.45	235.76	172.56	359.18	185.10
140.52	154.57	150.33	156.43	238.86	172.93	362.07	185.39
140.72	155.51	150.54	156.21	241.95	173.31	364.96	185.56
140.93	155.93	156.25	312.38	245.04	173.78	367.85	185.84
141.13	156.07	150.11	156.28	248.12	174.05		
141.33	156.01			251.19	174.28		
141.54	156.47	Series 7		254.26	174.72		
141.74	157.19	95.57	128.88	257.31	175.31		
141.95	157.50	99.14	131.31	260.36	175.60		

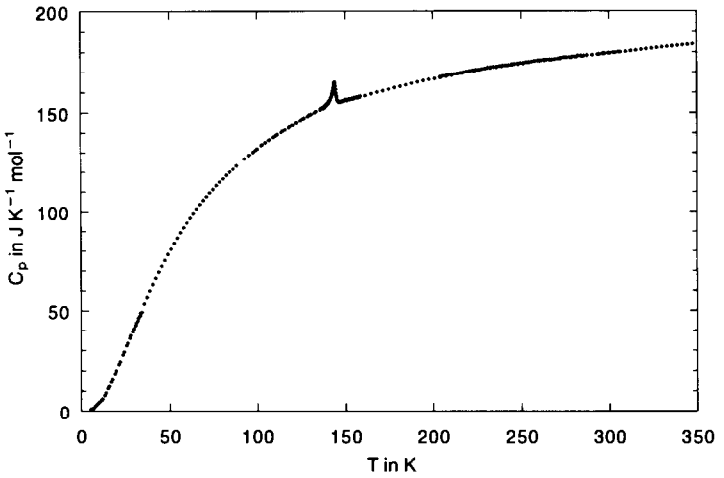

Fig. 1. Experimental molar heat capacities.

was observed in the stabilization periods; however in this series it is not the temperature drift which is anomalous, but the standard deviation of the time–temperature curve. Temperature drift and standard deviation are calculated for the second half of the stabilization periods. In series 1, the temperature is probably still falling in this half (total stabilization period 600 s), whereas in series 7 (total stabilization period 1200 s), the main temperature fall has already occurred, although the curve is not straight, resulting in a larger standard deviation. This suggests strongly that the sample is undergoing a slow reorganization between 147 and 210 K, starting very slowly at 147 K, gradually increasing and reaching its maximum at around 180 K.

In Fig. 2, the heat capacity data around the 146 K transition are plotted. To calculate the heat of transition, a baseline must be constructed. Takai et al. [13], whose data are discussed comparatively below, used a smooth baseline which starts to deviate from the experimental data at about 130 K and rejoins them at about 155 K. With this baseline, the transition not only shows a pre-effect, as we found, but also "tail" between 145 and 155 K. If, however, a discontinuity in the heat capacity around the transition is assumed (see Fig. 2), then the heat capacity data above the transition can be fitted perfectly with a straight line between 150 and 180 K, leaving a "tail" over only about two degrees. The onset of the transition remains, but with this baseline construction it starts a bit later than as reported by Takai et al. [13]: we find a clear start at around 140 K. The heat effect calculated using this baseline was found to be 30 ± 2 J mol^{-1}, lower than the value reported by Takai et al., 57 J mol^{-1}.

The low-temperature heat capacity data (between 5 and 30 K) cannot be fitted to the Debye T^3 law. We assumed that between 0 and 10 K this relation would be the best approximation, giving us a starting value for the

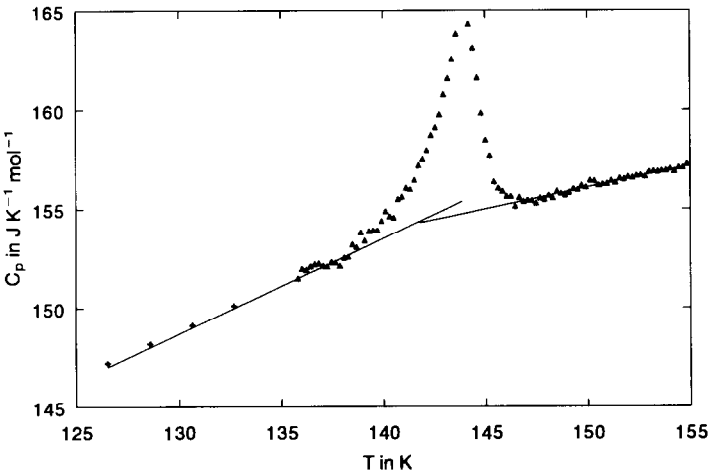

Fig. 2. Molar heat capacities around the transition region. The baselines used for calculating the heat of transition are drawn.

numeric integration procedure used to calculate the derived thermodynamic data, given in Table 3. When we compare our data with those of Takai et al [10], we find that they are the same within the combined errors of the calorimeters. For example, the value of $\Delta_0^{300}H^{\ominus}$ (Takai) is 39 890 J mol^{-1}; we obtained a value of 39 959 J mol^{-1}, the total difference in the heat capacity integrated over 300 K being only 0.17%. The same difference is found in the heat capacities at 300 K. The larger difference in $S(T) - S(0)$ (0.26%) must be attributed to the low-temperature extrapolation.

DISCUSSION

The data reported in this paper are in good agreement with those of Takai et al. [13]. The agreement between the studies shows that our results are not affected by water absorption. A common feature of these studies is the observation of a tail in the specific heat above the first-order phase transition. However, there is a discrepancy between the two studies in the width of this tailing effect, which is strongly dependent on the drawing of the baseline. In the present study, the tail is observed over only two degrees and may be related to the discommensuration mechanism predicted by McMillan [14]. In this respect the specific heat anomaly at 144 K would correspond to the lock-in transition below the second incommensurate phase. This **INC** phase would occur between 147 and 210 K, in accordance with a previous study [10], which revealed a kinetic behaviour of the transformation of the tetrahedron arrangement.

Specific heat measurements performed on single crystals [9] have indicated a sharp second anomaly which is not observed in the study of Takai et al. [13] nor in our work. Moreover, this second anomaly seems to be dependent on the pretreatment of the sample [8].

TABLE 3

Thermodynamic properties at selected temperatures for K_2ZnCl_4 ($M = 285.397\ g\ mol^{-1}$; $R = 8.3145\ J\ K\ mol^{-1}$; $\Phi_m^\ominus \overset{def}{=} \Delta_0^T S_m^\ominus - \Delta_0^T H_m^\ominus/T$)

T/K	$C_{p,m}^\ominus/R$	$\Delta S_m^\ominus/R$	$(\Delta H_m^\ominus/R)$/K	$\Phi_m^\ominus/R$
10	0.531	0.166	1.25	0.0416
20	2.495	1.050	15.16	0.2924
30	5.01	2.54	52.76	0.7816
40	7.53	4.33	115.5	1.4399
50	9.62	6.24	201.5	2.2078
60	11.41	8.16	307.1	3.0397
70	12.82	10.02	428.4	3.9049
80	13.99	11.81	562	4.7822
90	15.00	13.52	707	6.6584
100	15.86	15.14	862	6.5261
120	17.31	18.17	1194	8.2184
140	18.63	20.93	1553	9.840
160	19.02	23.45	1931	11.388
180	19.58	25.73	2317	12.857
200	20.05	27.82	2714	14.250
220	20.47	29.75	3119	15.572
240	20.82	31.54	3532	16.829
260	21.11	33.22	3951	18.026
280	21.35	34.80	4376	19.168
298.15	21.58	36.14	4765	20.162
300	21.60	36.28	4805	20.260
320	21.83	37.68	5239	21.305
340	22.05	39.01	5678	22.308
355	22.21	39.96	6010	23.034

Thus, the sequence of low-temperature phase transitions is as follows: firstly, a first-order phase transition is found at 146 K which seems to be independent of the thermal treatment, and secondly, above this transition a slow transformation of the $ZnCl_4$ tetrahedra takes place up to about 210 K. This transformation certainly depends on the thermal treatment, on the pretreatment of the sample and on its physical characteristics, such as crystal form (powder or single crystal). This behaviour of the modulation transformation in the low-temperature range can be interpreted as a memory effect due to the interaction between the modulation and lattice defects at room temperature.

This interaction is certainly responsible for the sequences of the phase transitions undergone by K_2ZnCl_4, Rb_2ZnCl_4, Rb_2ZnBr_4 and K_2SeO_4. The latter grows at room temperature in the high-temperature phase, in which there are no interaction modulation defects, and undergoes no phase transition below the three-fold superstructure. The other compounds grow in a modulated phase (**INC** or **C** phase) and exhibit phase transitions below

the three-fold superstructure. At room temperature, Rb_2ZnCl_4 and Rb_2ZnBr_4 are in the **INC** phase, where the interaction modulation defects are weak. They present a low-temperature **INC** phase which is clearly observed by Raman spectroscopy and heat capacity measurements. K_2ZnCl_4, however, grows in the three-fold superstructure where the interaction modulation defects are strong and the modulation undergoes a slow, time-dependent transformation by one or more **INC** states below room temperature. This transformation could proceed until very low temperatures are reached and this may explain the deviation of the data from the Debye law between 5 and 30 K. This deviation might also be caused by discommensurate moving or low-frequency excitation.

REFERENCES

1 N. Yamada and T. Ikeda, J. Phys. Soc. Jpn., 53 (1984) 2555.
2 A.C.R. Hogervorst and R.B. Helmhodt, Acta Crystallogr. Sect. B, 44 (1988) 120.
3 M. Quilichini, P. Bernede, J. Lefebvre and P. Schweiss, J. Phys. Condensed Matter, 2 (1990) 4543.
4 A. Hedoux, D. Grebille, J. Jaud and G. Godefroy, Acta Crystallogr. Sect. B, 45 (1989) 370.
5 B.K. Chaudhuri, K. Nomoto, T. Atake and H. Chihara, Phys. Lett., 79(4) (1980) 361.
6 E. Francke, M. le Postollec, J.P. Mathieu and H. Poulet, Solid State Commun., 33 (1980) 155.
7 K. Nomoto, T. Atake, B.K. Chaudhuri and H. Chikara, J. Phys. Soc. Jpn., 52 (1983) 3475.
8 K. Gesi, J. Phys. Soc. Jpn., 59 (1990) 416.
9 K. Gesi, J. Phys. Soc. Jpn., 61 (1992) 1225.
10 I. Noiret, A. Hedoux, Y. Guinet and M. Foulon, Europhys. Lett., 22 (1993) 265.
11 A. Hedoux, I. Noiret, Y. Guinet, G. Odou and J. Lefebvre, J. Chem. Phys., 97 (1992) 6181.
12 J.C. van Miltenburg, G.J.K. van den Berg and M.J. van Bommel, J. Chem. Thermodyn., 19 (1987) 1129.
13 S. Takai, T. Atake and K. Gesi, J. Phys. Chem. Solids, 54 (1993) 213.
14 W. L. McMillan, Phys. Rev. B, 14 (1976) 1496.